

Evidence for Two Distinct Populations of Type Ia Supernovae

Xiaofeng Wang^{1,2,*}, Lifan Wang^{2,3}, Alexei V. Filippenko⁴,
Tianmeng Zhang⁵, Xulin Zhao¹

¹Department of Physics, Tsinghua University, Beijing, 100084, China

²Mitchell Institute for Fundamental Physics and Astronomy, Texas A&M University, College Station, TX 77843, USA

³Purple Mountain Observatory, Nanjing, 201008, Jiangsu, China

⁴Department of Astronomy, University of California, Berkeley, CA 94720-3411, USA

⁵National Astronomical Observatory of China, Chinese Academy of Sciences, Beijing, 100012, China

*To whom correspondence should be addressed; E-mail: wang_xf@mail.tsinghua.edu.cn

Type Ia supernovae (SNe Ia) have been used as excellent standardizable candles for measuring cosmic expansion, but their progenitors are still elusive. Here we report that the spectral diversity of SNe Ia is tied to their birthplace environments. We find that those with high-velocity ejecta are substantially more concentrated in the inner and brighter regions of their host galaxies than are normal-velocity SNe Ia. Furthermore, the former tend to inhabit larger and more-luminous hosts. These results suggest that high-velocity SNe Ia likely originate from relatively younger and more metal-rich progenitors than normal-velocity SNe Ia, and are restricted to galaxies with substantial chemical evolution.

Type Ia supernovae (SNe Ia) are among the most energetic and relatively uniform stellar explosions in the Universe, and were used to discover its accelerating expansion (1, 2). They

are thought to originate from a thermonuclear explosion of an accreting carbon-oxygen white dwarf (WD) near the Chandrasekhar mass limit ($M_{\text{Ch}} \approx 1.4 M_{\odot}$) in a close binary system (3, 4). Two competing scenarios have been proposed for the progenitor systems: single-degenerate (SD) (5, 6) and double-degenerate (DD) models (4, 7). In the former, the mass-donating star could be a main-sequence (MS)/subgiant star (8), a red-giant star (RG; 9), or even a helium star (10, 11), while it is another WD in the latter scenario (4, 7). Recent results suggest that both scenarios are possible (12-18).

There is increasing evidence for spectral diversity among SNe Ia. Of particular interest are those showing higher expansion velocities as inferred from the blueshifted Si II 615 nm feature in optical spectra (19). These fast-expanding SNe Ia also generally exhibit a steep Si II temporal velocity gradient (20). This spectral difference in velocity or velocity evolution of the ejecta has been proposed to be a geometric effect of an asymmetric explosion (21, 22). Given a common origin for SNe Ia having different ejecta velocities, they should be found in similar stellar environments. This can be tested by examining SN positions in their hosts, the surface brightness at these locations, and the properties of their hosts.

We conducted such an analysis with a well-defined SN sample having 188 SNe Ia [see supporting online material (SOM) text S1] from the Lick Observatory Supernova Search (LOSS; 23). The SN Ia sample consists of 123 “Branch-normal” (spectroscopically normal) objects (24), 30 peculiar ones of the SN 1991bg variety (25), 13 peculiar ones like SN 1991T (26, 27), and 7 peculiar ones like SN 2002cx (28), with respective fractions of 65.4%, 16.0%, 6.9%, and 3.7% (Table S1). There are 15 SNe Ia (8.0% of all) that cannot be subclassified due to an absence of early-time spectra. We concentrate on the Branch-normal SNe Ia which are thought to be relatively uniform. We obtained the main parameters of the host galaxies from two large online astronomical databases: the NASA/IPAC Extragalactic Database (NED; 29) and HyperLeda (30).

The location of a SN in its host galaxy can be estimated by the radial distance of the SN from the nucleus (R_{SN}). Assuming that the galaxies are circular disks and only appear to have different major and minor axes due to their inclination, R_{SN} can be calculated if we know the position angle and the axial ratio of each galaxy. The radius of the galaxy (R_{gal}) is simply the semimajor axis at the 25.0 B -mag arcsec⁻² isophote. The ratio $R_{\text{SN}}/R_{\text{gal}}$ is then the fractional radial distance of the SN. For SNe Ia in elliptical galaxies, no tilt correction is applied because these galaxies can be regarded as spheroids. The typical host galaxy of our sample (Fig. S1) has a major axis of about 1.3'–1.4' and can be measured with a precision of $\sim 0.1'$. This results in a typical uncertainty of ~ 0.05 in the determination of $R_{\text{SN}}/R_{\text{gal}}$.

We measured the velocity of the Si II 615 nm line for 165 SNe Ia (out of 188) by using the published spectral datasets (31–33). We normalized this velocity to the maximum-light value with a series of templates of Si II velocity evolution established from well-observed SNe Ia, with a typical uncertainty of 300–400 km s⁻¹ (SOM text S1 and Fig. S2).

It is clear that Branch-normal SNe Ia with $v_{\text{Si II}} < 12,000$ km s⁻¹ (the normal-velocity group, NV) span a wide radial distribution, occurring at places from the innermost region to about 2–3 times the optical radius of the entire galaxy. In contrast, those with $v_{\text{Si II}} \geq 12,000$ km s⁻¹ (the high-velocity group, HV) are rarely found at large galactic radii (Fig. 1b). For example, only 3 out of the 40 HV SNe Ia are detected in regions with $R_{\text{SN}}/R_{\text{gal}} > 0.7$ (2 of which are in elliptical galaxies), whereas 14 ± 2 would have been expected at the detection rates of the NV SNe Ia (which are about $34 \pm 5\%$ at $R_{\text{SN}}/R_{\text{gal}} > 0.7$). Such a difference has a statistical significance of about 5σ , highlighting the paucity of HV SNe Ia in outskirts of galaxies. Binning the data in velocity space with an interval of about 2000 km s⁻¹ further shows a correlation between the ejecta velocity of SNe Ia and the locations in their host galaxies (see gray quadrangles in Fig. 1a).

To better understand such a birthplace vs. ejecta-velocity relation for SNe Ia, it is important

to know how the Si II velocity itself is distributed. Fig. 1c shows that most of the sample of Branch-normal SNe Ia clusters at velocities between 10,000 and 12,000 km s⁻¹, with a tail extending up to $\sim 16,000$ km s⁻¹. Such a velocity distribution can be fit by a double-Gaussian model. One component, with a stronger and narrower peak at 10,800 km s⁻¹, is responsible for the NV group, whereas the other component, with a weaker and broader peak at 13,000 km s⁻¹, accounts for the HV group. Adopting a velocity cut of $v_{\text{Si II}} = 12,000$ km s⁻¹ to divide these two groups puts 40 SNe Ia in the HV group and 83 in the NV group. Accordingly, we estimate the fraction of the HV population to be 1/3 of the Branch-normal sample and 1/5–1/4 of the entire SN Ia sample. Note that the Si II velocity distinction is not sharp between these two groups, so blending could occur to some extent. Nevertheless, this blending is small at larger velocities, and it will not affect the result that the SNe Ia with higher velocities tend to occur nearer the galaxy centers.

HV SNe Ia show the highest central concentration among the samples, with 90% occurring in regions within $R_{\text{SN}}/R_{\text{gal}} \leq 0.7$; this fraction is 66%, 77%, and 89% for NV SNe Ia, SNe II, and SNe Ibc, respectively (Fig.2). The contrast is even more significant when examining the distribution toward the galaxy center. We caution, however, that a higher fraction of CC SNe may be missing in the central regions of galaxies during LOSS because of their lower luminosity relative to SNe Ia.

A Kolmogoroff-Smirnoff (K-S) test finds a probability of 0.5% that HV and NV SN Ia groups have a similar radial distribution in galaxies. This probability further decreases to 0.1% if one increases the velocity cut dividing these two groups from 12,000 km s⁻¹ to 13,000 km s⁻¹. Possible selection effects in the radial distribution have been explored and none can account for such a significant discrepancy between HV and NV SN Ia groups (SOM text S2 and Figs. S3). Thus HV SNe Ia have higher metallicities and their progenitors are therefore less likely to be from the halo population that consists of old, metal-poor stars located far away from the

galactic center (34).

Because the radial distances give only a rough estimate of the properties of SN progenitors, more sophisticated methods are necessary to provide additional constraints. A simple statistic of the “fractional flux” allows a measurement of how SNe are distributed within their hosts (35). This can be achieved by measuring in the host-galaxy images the fraction of total galaxy light contained in pixels fainter than or equal to the light in the pixel at the location of the SN. The “fractional flux” was obtained with the SDSS $u'g'r'$ -band images (36) for 64 SNe Ia (39 NV + 25 HV), 102 SNe II, and 39 SNe Ibc of the entire SN sample (SOM text S3).

The surface brightness of SN II locations has an approximately linear distribution, roughly tracing the distribution of the light in their hosts (Fig. 3). SNe Ibc seem to be more concentrated in brighter regions of the host galaxies, consistent with the knowledge that they arise in larger star-forming regions that produce more-massive stars. Of the SN Ia sample, the locations of the HV group and the NV group track their hosts’ light differently, with a very low probability ($P = 0.04$ in u' , 0.07 in g' , and 0.08 in r') that they come from the same stellar populations. Figure 3 shows that the NV SN Ia locations are apparently fainter than those of CC SNe; the HV SN Ia distribution, on the other hand, is similar to the CC SN distribution.

The light radii and luminosities of galaxies in the HV sample and the NV sample also differ significantly (Fig. 4). A two-dimensional K-S test gives a probability of 0.5% that they come from the same population. The mean-light radius of the hosts estimated for these two groups is 20.67 ± 0.83 kpc for HV and 16.61 ± 0.67 kpc for NV. The mean absolute K -band magnitudes are -24.53 ± 0.13 mag (HV) and -24.17 ± 0.10 mag (NV), with the HV hosts being, on average, brighter by about 40%. In general, the HV SNe Ia tend to occur in larger and more luminous hosts, and the fraction found in galaxies with $R_{\text{gal}} < 15$ kpc is very low, 15% (versus 46% for the NV counterparts). This difference is not due to an observational bias because the host galaxies of these two groups do not show significantly different distributions in either morphologies or

redshifts (see SOM text S4 and Figs. S4 and S5).

Our analysis thus reveals significant differences in the progenitor environments of SNe Ia having different Si II velocities. The HV SNe Ia are much more concentrated in regions close to the galaxy center and in bright regions of their host galaxies, and they also tend to reside in larger and more luminous hosts relative to the NV group. It is generally accepted that all galaxies (on average) have metallicities that systematically decrease outward from their galactic centers, and that their global metallicities increase with galaxy size (39). Higher metallicity is therefore expected for the HV SN Ia progenitor population. Meanwhile, the fact that the surface brightness at HV SN Ia locations roughly traces the light of their host galaxies, as with CC SNe, suggests that the progenitor populations are relatively young. Thus, the HV SN Ia population may have a younger and more metal-rich progenitor system than the NV SN Ia population, and a larger initial MS mass of the exploding WD may be expected for the former due to the shorter evolutionary time needed before explosion.

Calculations of stellar evolution show that both stellar mass and metallicity have significant effects on the nature of C-O WDs that may become progenitors of SNe Ia. The maximum MS mass to form C-O WDs is found to increase significantly toward higher metallicity (40); stars with MS masses up to $8\text{--}9 M_{\odot}$ produce massive WDs ($\sim 1.1 M_{\odot}$) that can reach $1.4 M_{\odot}$ in a shorter time via mass transfer from a companion star. Thus, the HV SN Ia group might represent the young-population SNe Ia, corresponding to the “prompt” component with short delay times (41, 42), while the NV group may belong to the “older” component with long delay times. We note that 5 out of the 40 (12.5%) SNe Ia in the HV sample are in elliptical galaxies that are luminous (see Table S1 and Fig. S4) and massive. However, among these, some (e.g., SN 2002dj and SN 2000B) show dust structure and molecular gas (43, 44), suggestive of recent or ongoing star formation in them; they do not contradict the conclusion that HV SNe Ia likely arise from young stellar populations.

Having young and metal-rich progenitors may explain the numerous recent detections of circumstellar medium (CSM) signatures among HV SNe Ia. Time-variable absorption features of the Na I doublet (D1 589.6 nm and D2 589.0 nm), likely suggestive of changes in CSM ionization due to a variable SN radiation field, have been reported for a few SNe Ia such as SNe 2006X, 2007le, and 1999cl (*12, 45, 46*). A common feature of these SNe Ia is that they belong to the HV subclass (see Table S1). Additionally, the velocity structure of the line-of-sight Na I lines provides another possible diagnostic of CSM around SNe. A trend of blueshifts was found among SNe Ia based on a study of Na I absorption lines of a larger SN sample (*13*). It was noticed, however, that the SNe Ia with a blueshifted absorption feature generally have higher Si II velocities (*47*). This evidence is consistent with their systematically redder color around maximum light (perhaps due to additional CSM absorption) relative to the NV population (*19*), and it can be understood in terms of an empirical metallicity dependence of mass outflow (*48*). At higher metallicity, stars lose more mass and produce stronger outflows than their lower-metallicity counterparts. Thus, detection of abundant outflows in the vicinity of the HV SNe Ia is not unexpected.

The higher Si II velocity seen in HV SNe Ia may be related in part to an increase in stellar metallicity. As the metallicity increases in the C+O layer of the exploding WDs, the line-forming region moves toward shallower parts of the atmosphere because of an increased line opacity, leading to larger line velocities (*49*). In addition, the high-velocity Si II layers are perhaps formed due to the density increase caused by interaction between the SN ejecta and the material around the exploding WD, which could be an accretion disk or a filled Roche lobe (*50*). The angular variations in observing such an interacting system may explain the variation of the polarization across the Si II line (*51*) and its correlation with the ejecta velocity for HV SNe Ia (*22*). This is consistent with the result that the observed differences in some SNe Ia might be due to a projection effect (*21*). However, these data and analyses are insensitive to a separate

population of NV SNe Ia that is intrinsically different from HV SNe Ia.

The dependence of SN Ia ejecta velocity on progenitor environment could be relevant when using SNe Ia as cosmological yardsticks, because the HV and NV populations have different colors around maximum light (*19*) and their ratio may change with redshift. The observed relative fraction of the HV and NV population might become smaller at great distances due to a decrease in the HV SN Ia rate in low-metallicity environments and the increased difficulty of spectroscopically classifying SNe in the central regions of distant galaxies.

References and Notes

1. A. G. Riess, et al., *Astron. J.* **116**, 1009 (1998).
2. S. Perlmutter, et al., *Astrophys. J.* **517**, 565 (1999).
3. K. Nomoto, *Astrophys. J.* **253**, 798 (1982).
4. I. Iben, Jr. & A. V. Tutukov, *Astrophys. J. Suppl. Ser.* **54**, 335 (1984).
5. K. Nomoto, K. Iwamoto, & N. Kishimoto, *Science* **276**, 1378 (1997).
6. P. Podsiadlowski, P. Mazzali, P. Lesaffre, Z. Han, & F. Förster, *N. Astro. Rev.* **52**, 381 (2008).
7. R. F. Webbink, *Astrophys. J.* **277**, 355 (1984).
8. E. P. J. van den Heuvel, D. Bhattacharya, K. Nomoto, & S. A. Rappaport, *Astron. Astrophys.* **262**, 97 (1992).
9. U. Munari & A. Renzini, *Astrophys. J.* **397**, L87 (1992).
10. B. Wang & Z. W. Han, *Astron. Astrophys.* **515**, A88 (2010).
11. S.-C. Yoon & N. Langer, *Astron. Astrophys.* **412**, L53 (2003).
12. F. Patat, et al., *Science* **317**, 924 (2007).
13. A. Sternberg, A. Gal-Yam, & J. D. Simon, *Science* **333**, 856 (2011).
14. P. Nugent, et al., *Nature* **480**, 344 (2011).
15. W. Li, et al., *Nature* **480**, 348 (2011).
16. J. Bloom, et al., *Astrophys. J.* **744**, L17 (2012).

17. P. Brown, et al., *Astrophys. J.* **753**, 22 (2012).
18. B. Schaefer & A. Pagnotta, *Nature* **481**, 164 (2012).
19. X. Wang, et al., *Astrophys. J.* **699**, L139 (2009).
20. S. Benetti, et al., *Astrophys. J.* **623**, 1011 (2005).
21. K. Maeda, et al., *Nature* **466**, 82 (2010).
22. J. R. Maund, et al., *Astrophys. J.* **725**, L167 (2011).
23. J. Leaman, W. Li, R. Chornock, & A. V. Filippenko, *Mon. Not. R. Astron. Soc.* **412**, 1419 (2011).
24. D. Branch, A. Fisher, & P. Nugent, *Astron. J.* **106**, 2383 (1993).
25. A. V. Filippenko, et al., *Astron. J.* **104**, 1543 (1992).
26. A. V. Filippenko, et al., *Astrophys. J.* **384**, 15 (1992).
27. M. M. Phillips, et al., *Astron. J.* **103**, 1632 (1992).
28. W. Li, et al., *Publ. Astron. Soc. Pac.* **115**, 453 (2003).
29. <http://ned.ipac.caltech.edu/> .
30. <http://leda.univ-lyon1.fr/> .
31. S. Blondin, et al., *Astron. J.* **143**, 126 (2012).
32. J. M. Silverman, et al., *Mon. Not. R. Astron. Soc.* **425**, 1789 (2012).
33. T. Matheson, et al., *Astrophys. J.* **135**, 1598 (2008).

34. K. M. Gilbert, et al. *Astrophys. J.* **652**, 1181 (2006).
35. A. S. Fruchter, et al., *Nature* **441**, 463 (2006).
36. D. G. York, et al., *Astron. J.*, **120**, 1579 (2000).
37. D. N. Spergel, et al., *Astrophys. J. Suppl. Ser.* **170**, 377 (2007).
38. D. J. Schlegel, D. P. Finkbeiner, & M. Davis, *Astrophys. J.* **500**, 525 (1998).
39. R. B. C. Henry & G. Worthey, *Publ. Astron. Soc. Pac.* **111**, 919 (1999).
40. H. Umeda, et al., *Astrophys. J.* **513**, 861 (1999).
41. E. Scannapieco & L. Bildsten, *Astrophys. J.* **629**, L85 (2005).
42. F. Mannucci, M. Della Valle, & N. Panagia, *Mon. Not. R. Astron. Soc.* **370**, 773 (2006).
43. P. Goudfrooij, L. Hansen, H. E. Jorgensen, et al. *Astron. Astrophys. Suppl. Ser.* **105** 341 (1994).
44. L. M. Young, et al., *Mon. Not. R. Astron. Soc.* **414**, 940 (2011).
45. J. D. Simon, et al., *Astrophys. J.* 702, 1157 (2009).
46. S. Blondin, et al., *Astrophys. J.* 693, 207 (2009).
47. R. J. Foley, et al., *Astrophys. J.* **752**, 101 (2012).
48. P. R. Wood, *ASP Conf. Ser.* **404**, 255 (2009).
49. E. J. Lentz, et al., *Astrophys. J.* **530**, 966 (2000).
50. C. Gerardy, et al., *Astrophys. J.* **607**, 391 (2004).
51. L. Wang, D. Baade, & F. Patat, *Science* **315**, 212 (2007).

Acknowledgments.

We thank I. Dominguez for helpful discussions and C. WU for assistance with the SDSS images. This work is supported by the National Natural Science Foundation of China (NSFC grants 11073013, 11178003), the Major State Basic Research Development Program (2009CB824800), and the Foundation of Tsinghua University (2011Z02170). The work of L.W. is supported by NSF grant AST-0708873. A.V.F. is grateful for financial assistance from NSF grant AST-1211916, the TABASGO Foundation, and the Christopher R. Redlich Fund. We dedicate this paper to the memory of our dear friend and colleague, Weidong Li, whose unfailing dedication to the Lick Observatory Supernova Search made this work possible; his premature, tragic passing has deeply saddened us.

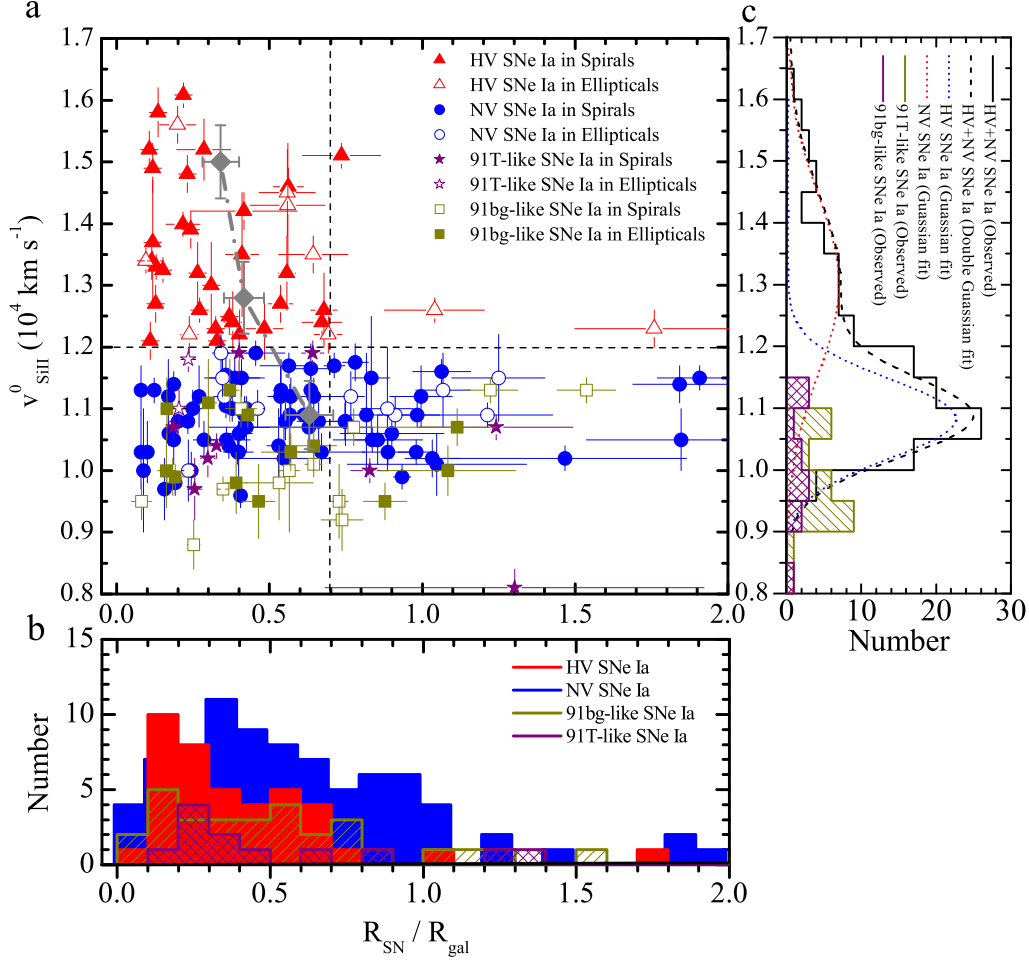


Fig. 1: Relations between the Si II velocity of SNe Ia and the birth location in their host galaxies. **a**, The Si II velocity obtained around B -band maximum light ($v_{\text{Si II}}^0$, ordinate) as compared to the fractional radial distance in the host galaxy ($R_{\text{SN}}/R_{\text{gal}}$, abscissa) for 165 SNe Ia. The Branch-normal SNe Ia with $v_{\text{Si II}}^0 \geq 12,000 \text{ km s}^{-1}$ (HV group), those with $v_{\text{Si II}}^0 < 12,000 \text{ km s}^{-1}$ (NV group), SN 1991T-like SNe, and SN 1991bg-like SNe are shown by red triangles, blue dots, purple stars, and dark-gray squares, respectively. The SNe Ia in spiral and elliptical/lenticular galaxies are represented with filled and open symbols, respectively. The gray quadrangles show the radial distances averaged in binned velocity space, which are 0.63 ± 0.08 in $9,000\text{--}12,000 \text{ km s}^{-1}$, 0.42 ± 0.06 in $12,000\text{--}14,000 \text{ km s}^{-1}$, and 0.34 ± 0.06 in $\sim 14,000\text{--}16,000 \text{ km s}^{-1}$, respectively. The horizontal and vertical dashed lines mark the place with $v_{\text{Si II}} = 12,000 \text{ km s}^{-1}$ and with $R_{\text{SN}}/R_{\text{gal}} = 0.7$. **b**, The number distribution of the fractional radial distance. The red and blue areas are for the HV and NV groups of SNe Ia. The purple and dark-gray areas are for the SN 1991T-like and SN 1991bg-like SNe Ia. **c**, The number distribution of near-maximum-light Si II velocity. A double Gaussian function is used to fit the distribution of 123 Branch-normal (HV + NV) SNe Ia. Red and blue curves are for the high-velocity and normal-velocity components, with respective peaks centered at $13,000 \text{ km s}^{-1}$ and $10,800 \text{ km s}^{-1}$. The black curve represents the combined result of these two components.

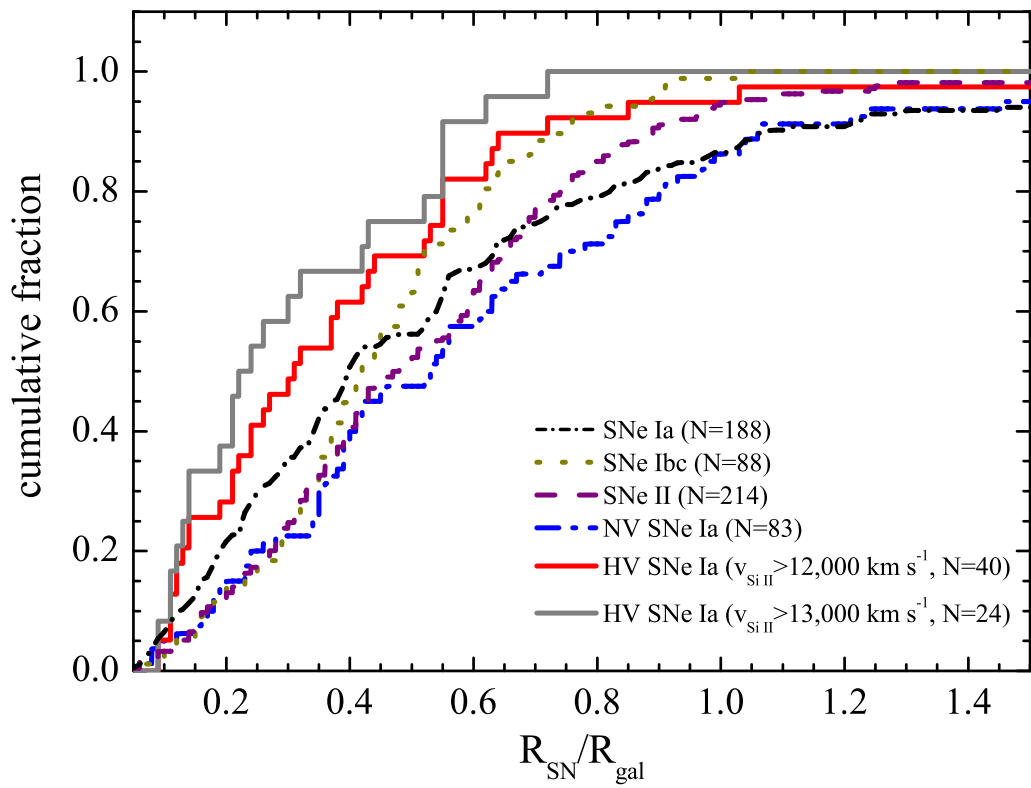


Fig. 2: A plot of the cumulative fraction of our SN samples (HV SNe Ia, NV SNe Ia, SNe II, and SNe Ibc). The gray solid curve represents the distribution of SNe Ia with $v_{\text{Si II}} > 13,000 \text{ km s}^{-1}$.

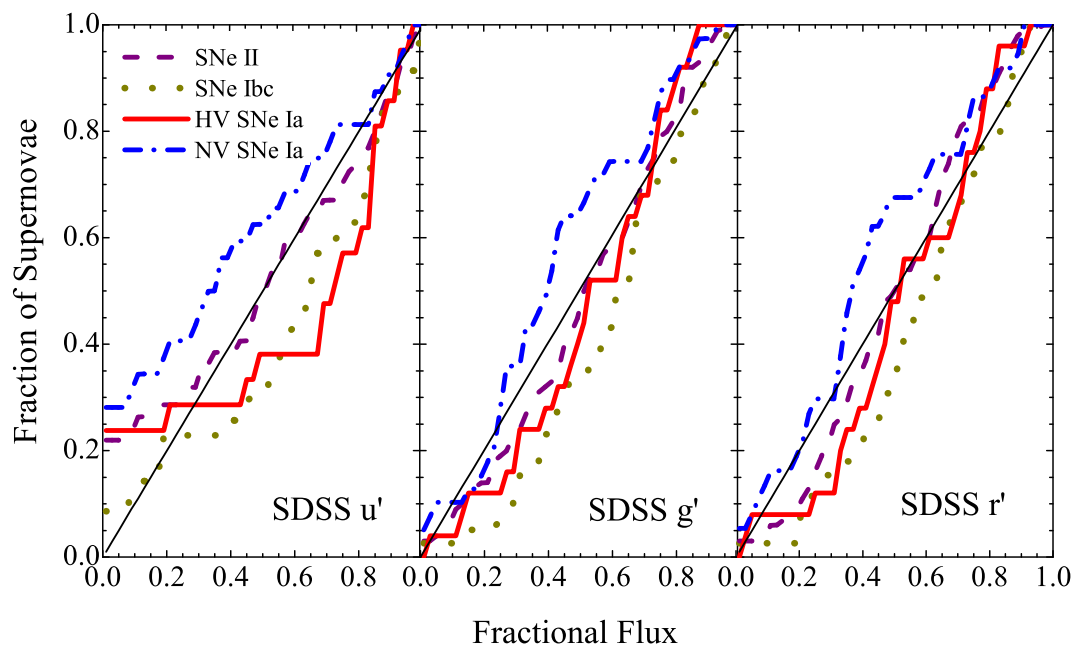


Fig. 3: Histogram distribution of the fractional flux of the host-galaxy light at the location of SN explosions in the u' (left panel), g' (middle panel), and r' (right panel) bands. The diagonal black lines represent the case that the SN progenitors follow exactly the distribution of galaxy light. The HV SN Ia population differs significantly from the NV SN Ia population at the SN location (with a respective probability of 3.8% in u' , 6.8% in g' , and 8.3% in r' that the SNe come from the same radial distribution), but seems to have a distribution similar to those of SNe II and SNe Ibc..

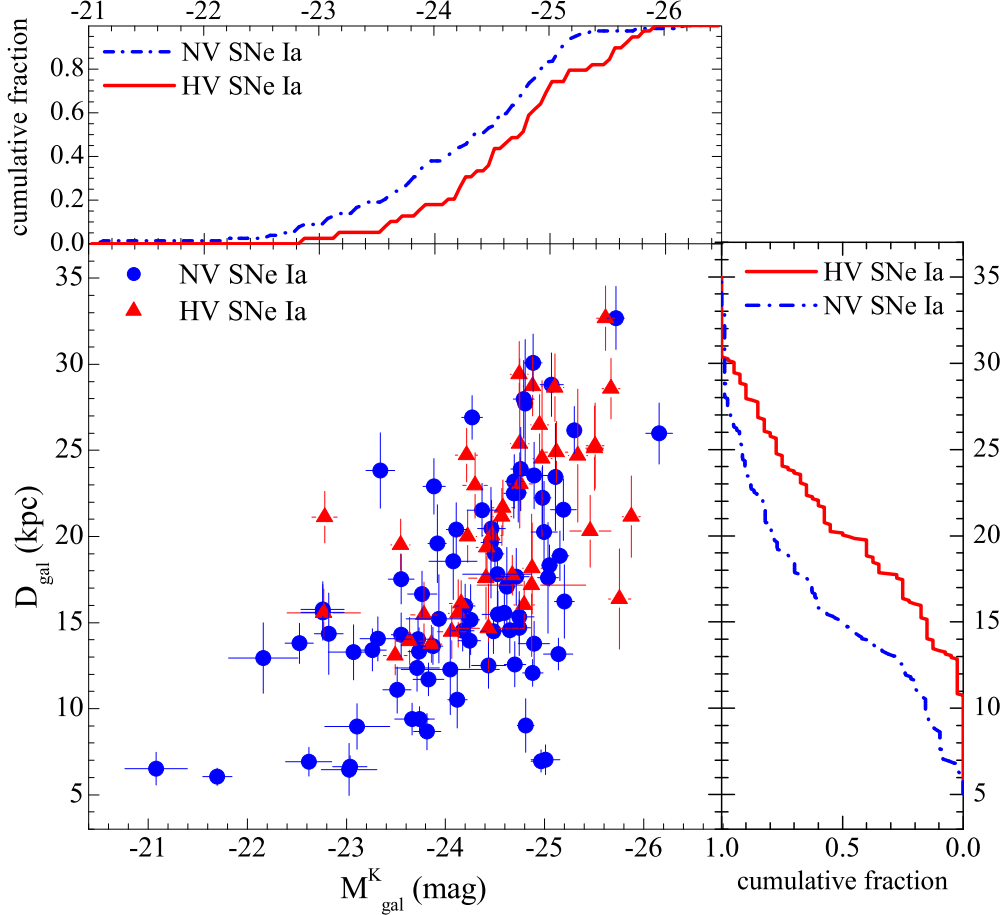


Fig. 4: A comparison of the physical sizes (B -band light radius at $25 \text{ mag arcsec}^{-2}$ isophote) and absolute K -band magnitude distributions of the SN hosts. These two parameters have been derived by adopting $\Omega_m = 0.27$, $\Omega_\Lambda = 0.73$, and $H_0 = 73 \text{ km s}^{-1} \text{ Mpc}^{-1}$ (37). Foreground Galactic absorption corrections (38) have been applied to the absolute magnitudes. In the main panel, the high-velocity SN Ia hosts are represented as red triangles, and the normal-velocity SN Ia hosts as blue dots. The absolute magnitudes of the hosts are shown on the abscissa, and the lengths of the semimajor axes of the hosts on the ordinate. The plot is then projected onto the two side panels where a histogram is displayed for each host population in each of the dimensions, absolute magnitude and semimajor axis.

Supporting Online Material

S1. The Supernova Sample

The SN sample used in our study is the "season-optimal" subsample from the Lick Observatory Supernova Search (LOSS), found over the interval 1998–2008 (23). This subsample contains 499 SNe that were discovered only during (not prior to) the active monitoring period of their host galaxies, with those in small early-type and edge-on spiral galaxies further excluded (see Table 4 of Ref. 23). Fig. S1 shows the typical host galaxies of the "season-optimal" subsample used in our study. Among the 499 SNe, 188 are SNe Ia (37.7%), 214 are SNe II (43.1%), 88 are SNe Ibc (17.6%), and 9 have no known spectroscopic classification (1.8%). These fractions of different SN types are fully consistent with those from the full "optimal" sample (726 in total, of which 284 are SNe Ia) used for the final rate calculations for nearby SNe (52), arguing against a possible bias in the sample selection. The main advantage of adopting the smaller "season-optimal" subsample is that the discovered SNe are generally at a relatively young phase, allowing accurate, timely spectroscopic classifications of them. This is particularly important for the identification of spectral diversity among SNe Ia.

The ejecta velocity can be measured from the absorption minimum of the blueshifted Si II 635.5 nm line, which is one of the strongest features in early-time optical/near-infrared spectra of SNe Ia and suffers from little blending with other features. In order to measure an accurate expansion velocity from the Si II lines, we smoothed the observed spectrum with a locally weighted scatter-plot smoothing method (53) to avoid taking a dip of a noise spike in the data as a local absorption minimum. As shown in the inset of Fig. S2, the wavelength of the minimum in the smoothed spectrum (λ_{min}) is used to calculate the expansion velocity using the special-relativistic formula. We further compare these velocities obtained within about one week from

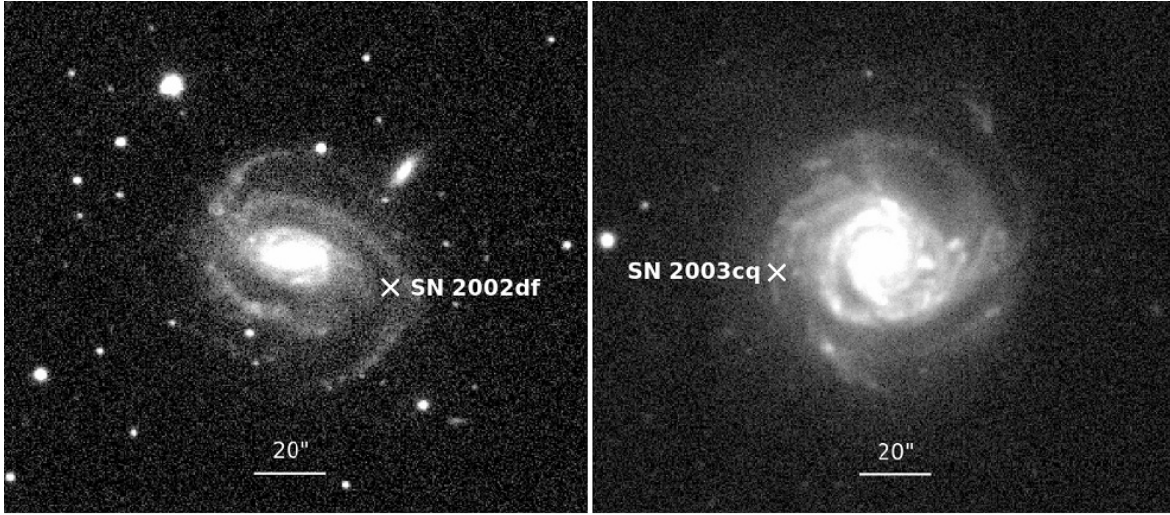


Fig. S1: Typical galaxies in the sample. Left: SDSS g' -band image of the host galaxy MCG-1-53-6 of SN 2002df, a member of the NV population of SNe Ia. Right: SDSS g' -band image of the host galaxy NGC 3978 of SN 2003cq, a member of the HV population of SNe Ia. Both images have a size of $2.8' \times 2.5'$.

maximum light to templates of Si II velocity evolution to determine the corresponding values at maximum light, $v_{Si II}^0$ (see Fig. S2). These comparison templates are established from some well-observed objects with published spectral data (19, 31-33, and references therein). The values of $v_{Si II}^0$ used in this study are listed in Table S1, with a typical uncertainty of about $300\text{-}400 \text{ km s}^{-1}$, depending on the number, epoch, and quality of the available spectra.

Following the classification scheme proposed by Wang et al. (19), we divide the 188 SNe Ia into five groups: high velocity (HV), normal velocity (NV), overluminous SN 1991T-like (91T), subluminous SN 1991bg-like (91bg), and the extremely peculiar SN 2002cx-like (02cx) SNe Ia, with respective relative fractions of 21.2%, 44.1%, 6.9%, 16.0%, and 3.7%. (8.1% of SNe Ia could not be classified due to the absence of early-time spectra.) The HV:NV ratio, derived with the "season-optimal" subsample, may suffer some effects from the excluded sample. However, these effects cannot be directly addressed because we do not have early-time spectra of most of the excluded SNe and we were thus not able to subclassify them. The spectral data used for the

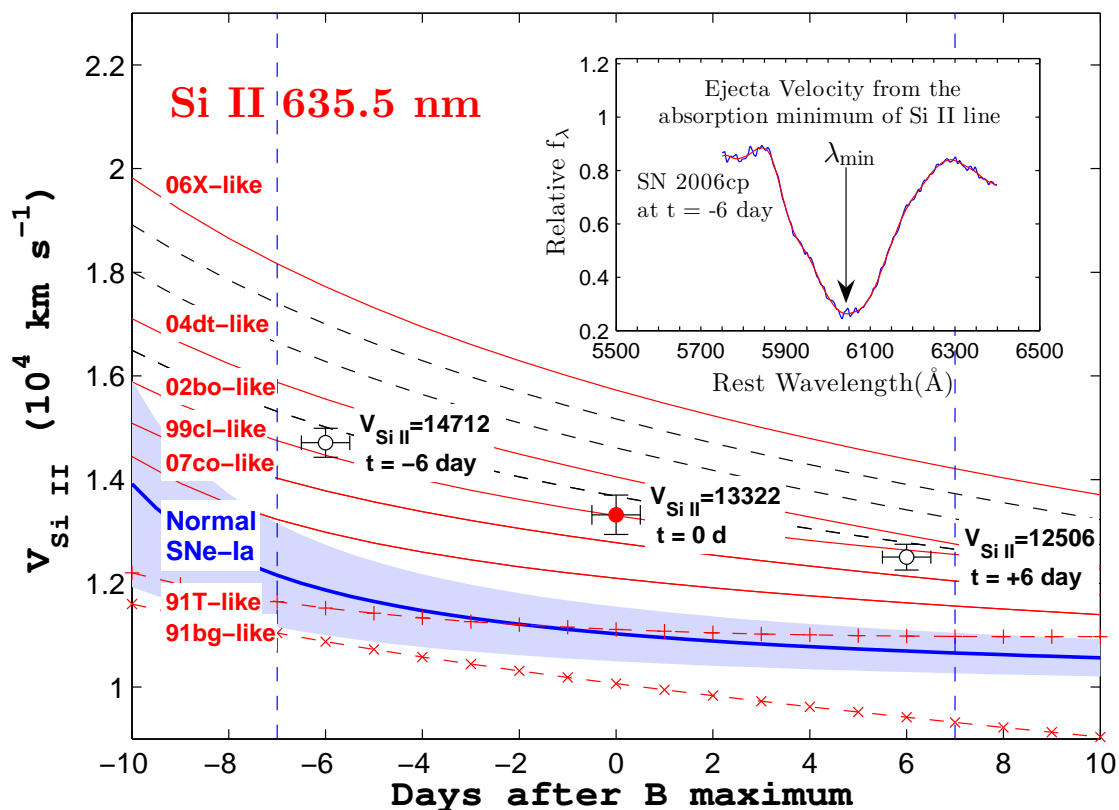


Fig. S2: An example of the Si II velocity measurement and normalization used in this study. The absorption feature shown in the inset window is Si II 635.5 nm from a spectrum of SN 2006cp at $t = -6$ day from maximum light. The observed spectrum is the solid black curve, the locally weighted scatterplot smoothed spectrum is the solid red curve, and the absorption minimum is indicated by the position indicated by the down arrow. The measured velocities (represented by the black filled dots) are then normalized to the value at maximum light (indicated by the red filled dot) by comparing with the template curves of the well-observed SNe Ia. The blue curve shows the mean evolution of NV SNe Ia, and the gray region represents the 1σ uncertainty; the red curves are part of the HV sample; the dashed-plus and dashed-cross lines illustrate the evolution of the mean velocity for SN 1991T-like and SN 1991bg-like events, respectively. These templates are established with the published spectral data from the literature (2–4). The black dashed curves represent the interpolated HV templates from the neighboring observed ones, with an assumption of proportional change.

subclassifications in this study are based primarily on the datasets published by the Center for Astrophysics Supernova Program (31, 33) and the Berkeley Supernova Program (32). For some objects the spectral parameters are taken from the IAU Circulars.

Table S1 lists the observed parameters as well as the classifications of the 188 SNe Ia. The meaning of each column is as follows: Column (1), the SN name; Column (2), the host-galaxy name; Column (3), the recession velocity (v) in the reference frame of the cosmic microwave background (CMB) when $v > 3000 \text{ km s}^{-1}$, or for a self-consistent Virgo-centric infall vector of 220 km s^{-1} when $v < 3,000 \text{ km s}^{-1}$, using the procedure given at the NASA Extragalactic Database (NED); Column (4), the host-galaxy numerical Hubble type, or "T" type (54); Column (5), the host-galaxy absolute K -band magnitude taken from The 2MASS Redshift Survey (55), dereddened by the Galactic reddening using the full-sky maps of dust infrared emission (38) and the Cardelli et al. reddening law with $R_V = 3.1$ (56); Column (6), the host-galaxy physical radius at the $25.0 B$ -mag arcsec $^{-2}$ isophote; Column (7), the deprojected galactocentric distance of the SN in its host galaxy, in units of the galaxy radius R_{gal} ; Column (8), the velocity of Si II line measured around maximum light, and its uncertainty; Columns (9)-(11), the u' -, g' -, and r' -band fractional fluxes, measured with the SDSS (36) images (57), representing the sum of counts registered in all pixels with fewer counts than measured at the SN location divided by the sum of all counts associated with the galaxy (35, 58); and Column (12), the SN Ia subtype.

S2. Some Selection Effects in the Determination of the Radial Distance

In calculating the SN relative distance, we assumed that galaxies are circular disks and that they exhibit different major and minor axes only because of different inclinations. This assumption can be used to derive the deprojected radial distance of the SNe in spiral galaxies with an intermediate inclination angle (e.g., $< 70^\circ$). For galaxies with large inclination angles, such a tilt

correction may cause large uncertainties in an attempt to derive the deprojected distance. As an alternative, we can also make an assumption of spheroids for all of the galaxies. Based on the projected radial distance, we reanalyzed the data and found that the HV SN Ia sample is still highly concentrated near the galaxy center relative to the NV sample, with a K-S probability of 0.3% that they come from the same parent population.

We further considered possible selection effects that may bias the radial distribution of the HV and NV SNe Ia, which can arise from differences in SN luminosity and size of the host galaxy. For example, brighter SNe are more easily detectable in the central regions of galaxies than fainter SNe. In Figure S3, we compared the distribution of the V-band magnitudes M_{max}^V , corrected for Galactic reddening, for the HV and NV SN Ia samples. The mean value and the distribution of M_{max}^V are found to be comparable for these two samples. This indicates that the selection effect due to the different luminosity distributions of HV and NV SNe Ia should not have a significant bias on the radial distribution in their host galaxies.

According to the analysis of the LOSS SN sample (23), there is a higher probability that the SNe tend to be missed in the central regions of smaller galaxies relative to that of larger galaxies. We further examined this possible selection effect by excluding the smaller galaxies from our analysis. Restricting the sample used in the analysis to the SNe Ia with major axis of the host galaxy greater than 1.0' (a total of 96) and 1.3' (a total of 56), we found that the differences in radial distributions between the HV and NV subsamples are still statistically significant, with K-S probabilities of 0.4% and 5.7% that they come from the same population.

The above analysis indicates that the concentration of HV SNe Ia in the central regions of galaxies cannot be explained with any known selection effects, so it seems to be a property intrinsic to these objects.

S3. Measurements of the Fractional Flux at the SN Location

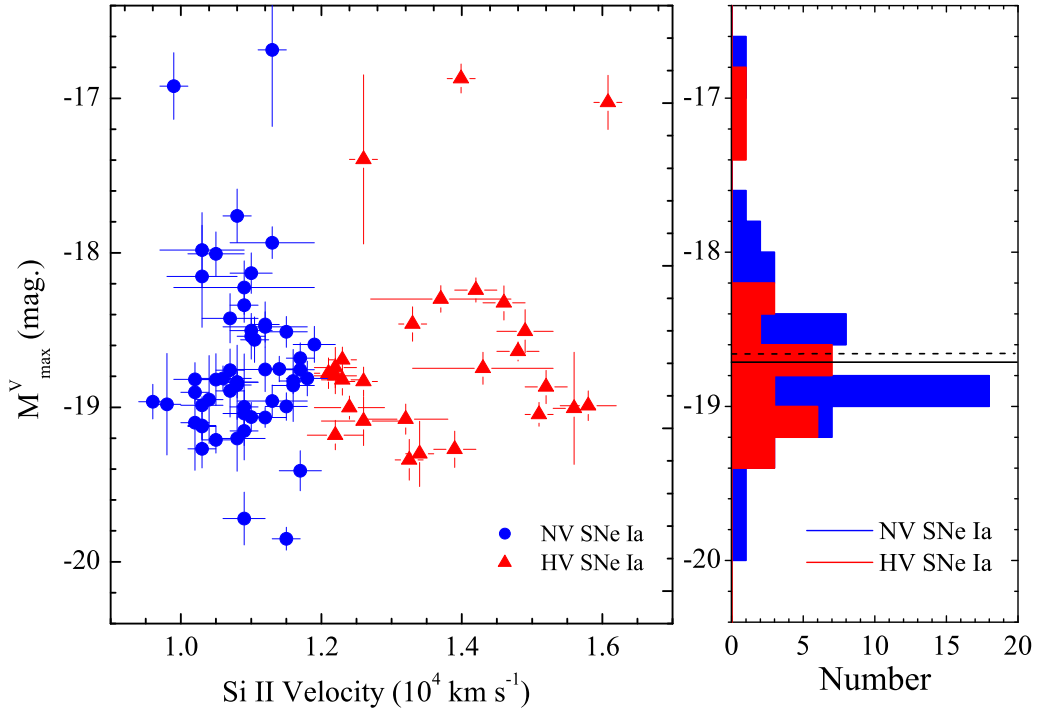


Fig. S3: Left panel: The V-band absolute magnitudes, corrected for Galactic reddening, plotted as a function of the Si II velocity around maximum light. Right panel: Histograms of V-band absolute magnitudes for the HV and NV subclasses of SNe Ia. Two vertical lines in the panel mark the respective mean values of the absolute magnitudes for the NV (solid) and HV (dashed) SNe Ia, which are 18.71 ± 0.08 mag and 18.64 ± 0.12 mag. A K-S test rejects the hypothesis with a probability of 99.6% that these two SN Ia populations have different peak luminosities.

The fractional flux is measured in host-galaxy images as the fraction of total host light in pixels fainter than or equal to the light in the pixel at the location of the SN (35). Were the SNe of different types to exactly track the host-galaxy light, their histograms would follow the diagonal line. This parameter is independent of galaxy morphology and provides a better way to quantify the correlation between SNe and the light of their hosts. The host-galaxy images in our analysis were taken from the SDSS DR 6 (56), which includes 54-s exposures in the Sloan filter set. To avoid possible contamination by residual light from the SNe, we excluded those images in which the SDSS observation of the host was made during the period from 1 month before to 12 months after the SN detection. The SDSS u'g'r'-band images were used for the measurements; they are available for 25 HV SNe Ia, 39 NV SNe Ia, 39 SNe Ibc, and 102 SNe II.

Following Ref. (57), we identify the pixels with host-galaxy light by selecting contiguous pixels having signal-to-noise ratios greater than 1. Before that, the foreground stars were masked out and the enclosed pixel values were replaced with the mean of pixel values around the mask perimeter. From the distribution of pixel values of the galaxy light in the SDSS u'g'r' bands and the corresponding values at the SN location, we calculate the fractional fluxes. All of the results are listed in columns (10)-(12) of Table S1. Note that the u'-band fractional flux may suffer larger uncertainties because the SDSS images are not deep enough in this band to allow accurate measurements.

S4. Redshift and Morphology of the Host Galaxies

Figure S4 shows the redshift distribution of the host galaxies. The mean redshift distribution is estimated as $z = 0.0240$ for the HV SNe Ia and 0.0217 for the NV SNe Ia; the HV SN Ia hosts are, on average, at slightly larger distances. Such a small difference cannot account for the

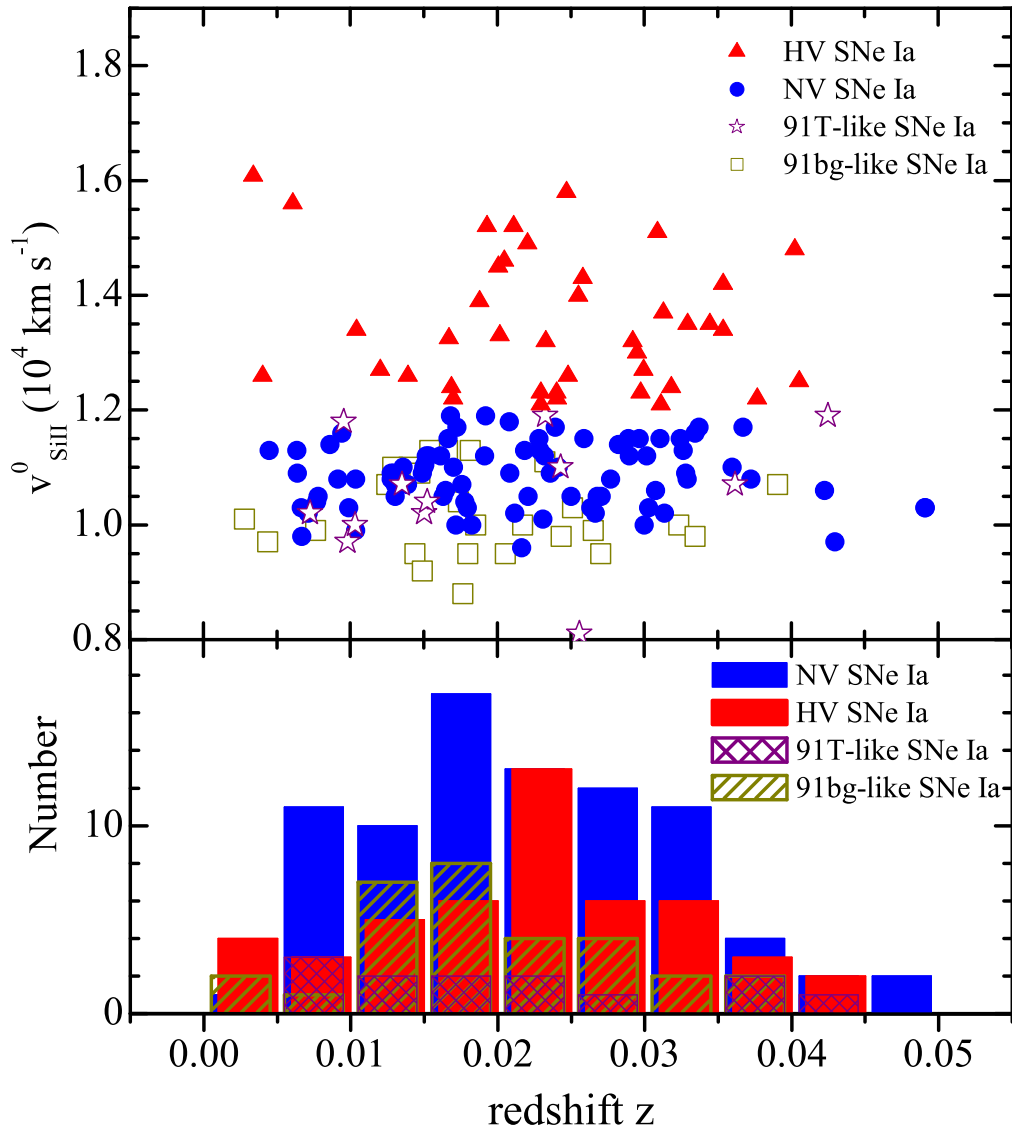


Fig. S4: A plot of the Si II velocities of SNe Ia near maximum light and the redshift of their host galaxies. In the upper panel, the HV SN Ia hosts are represented as red triangles, the NV SN Ia hosts as blue dots, the 91T-like hosts as purple stars, and the 91bg-like hosts as dark-yellow squares. The lower panel shows a histogram for the redshift distribution of the hosts of different types. The mean redshift for the HV SN Ia sample is 0.024, comparable to that of the NV sample (mean value 0.022)..

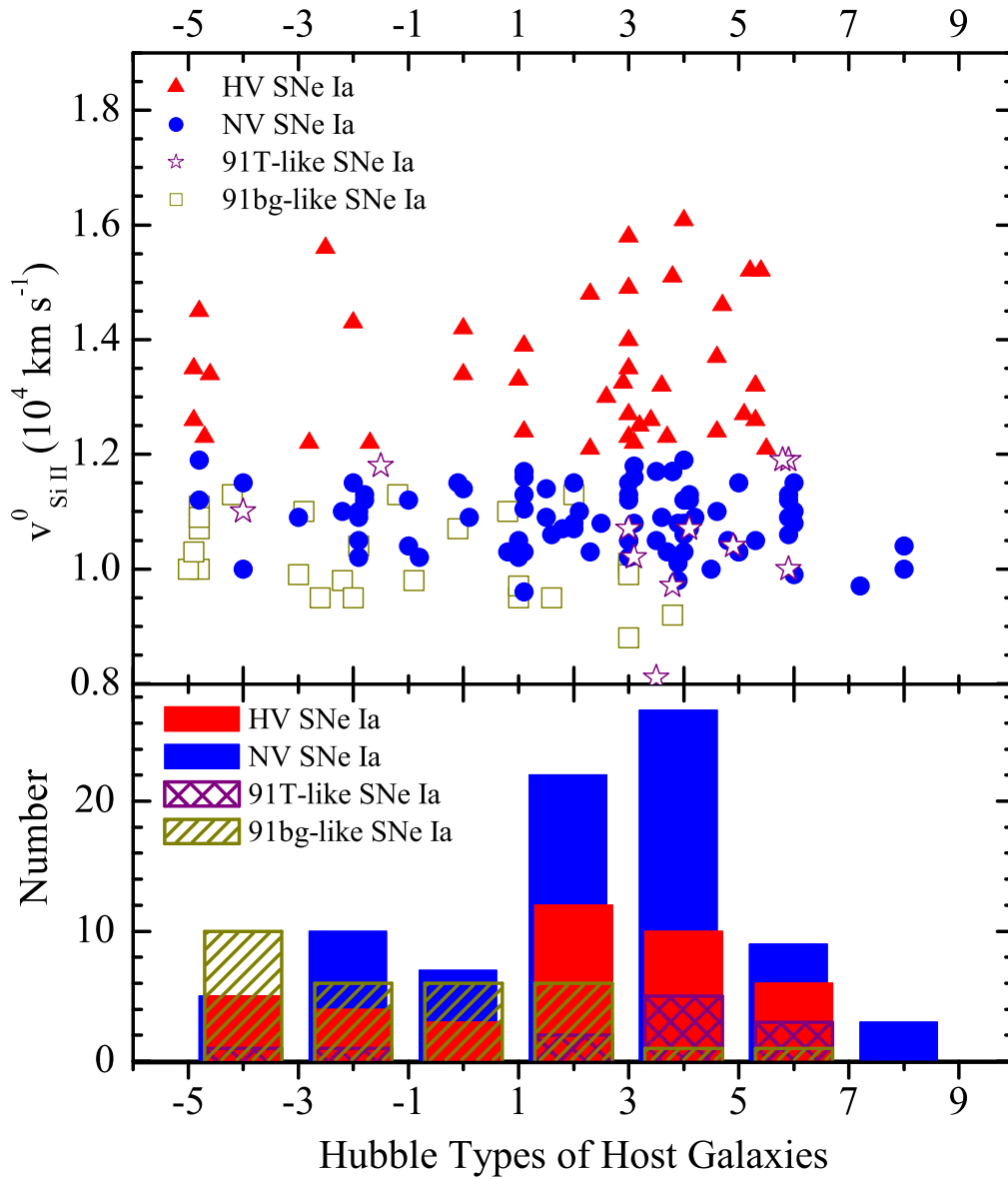


Fig. S5: A plot of the Si II velocities of SNe Ia near maximum light and the numerical Hubble types of their host galaxies. The symbols are the same as in Fig. S4. The plot is then projected onto the lower panel, where a histogram distribution is displayed for each Hubble type of the host populations. The K-S test gives a probability of 70% that the HV hosts and NV hosts have the same morphological distribution.

paucity of the HV SNe Ia in smaller galaxies, as the mean absolute B -band magnitude and the major axis of the host galaxies are found to increase by only ~ 0.08 mag and ~ 0.8 kpc from $z = 0.0217$ to 0.0240 . The Hubble type ("T" type) of the host galaxies of the HV and NV SN Ia samples is also compared in Figure S5. A K-S test gives a probability of 70% that these two samples have a similar morphology distribution, indicating that the differences in light radii and luminosity of galaxies seen in Figure 4 are not due to an observational bias.

References

52. W. D. Li, et al. *Mon. Not. R. Astron. Soc.* **412**, 1473 (2011).
53. W. S. Cleveland, *J. Am. Statist.* **74**, 368 (1979).
54. G. de Vaucouleurs, A. de Vaucouleurs, H. G. Corwin, R. J., Buta, G. Paturel, and P. Fouque, *Third Reference Catalogue of Bright Galaxies* (New York: Springer-Verlag) (1991).
55. J. P. Huchra, et al. *Astrophys. J. Suppl. Ser.* **199**, 26 (2012).
56. J. A. Cardelli, G. C. Clayton, & J. S. Mathis, *Astrophys. J.* **345**, 245 (1989).
57. J. K. Adelman-McCarthy, et al. *Astrophys. J. Suppl. Ser.* **175**, 297 (2000).
58. P. L. Kelly, R. P. Kirshner, & M. Pahre, *Astrophys. J.* **687**, 1201 (2008).

Table S1: Relevant Parameters of the SN Ia Sample

SN	Galaxy	v_{3k} (km s ⁻¹)	Galaxy Type	M_K (mag.)	R_{gal} (kpc)	R_{SN}/R_{gal}	$V_{Si II}^0$ (10 ⁴ km s ⁻¹)	f_u	f_g	f_r	SN Type*
1998de	NGC 252	4619	-1.2	-24.98(14)	14.43(125)	1.54(10)	1.13(02)	Iabg
1998dk	UGC 139	3609	5.1	-22.45(19)	15.56(138)	0.13(01)	1.27(03)	0.88	0.88	0.83	IaH
1998ef	UGC 646	5019	2.9	-23.78(14)	15.46(187)	0.15(02)	1.33(02)	IaH
1998es	NGC 632	2868	-1.5	-22.89(23)	8.86(109)	0.23(02)	1.18(02)	0.64	0.48	0.45	IaT
1999aa	NGC 2595	4572	4.9	-24.34(15)	28.78(214)	0.33(01)	1.04(02)	0.37	0.60	0.52	IaT
1999ac	NGC 6063	3098	5.9	-22.60(22)	10.49(119)	0.83(06)	1.00(02)	0	0.07	0.07	IaT
1999bh	NGC 3435	5295	3.0	-23.58(13)	18.00(144)	0.25(02)	0.88(04)	0.62	0.62	0.54	Iabg
1999by	NGC 2841	841	3.0	-24.68(23)	13.02(486)	0.64(03)	1.01(02)	0.50	0.93	0.87	Iabg
1999cl	NGC 4501	1217	3.4	-24.87(55)	17.17(414)	0.27(02)	1.26(02)	0.44	0.51	0.48	IaH
1999cp	NGC 5468	3112	6.0	-22.76(22)	15.76(161)	0.75(02)	1.08(04)	IaN
1999da	NGC 6411	3748	-4.8	-24.45(18)	16.00(235)	1.11(13)	1.07(03)	0.13	0.10	0.02	Iabg
1999dg	UGC 9758	6782	-2.0	-24.65(10)	16.21(147)	0.20(02)	...	0.81	0.41	0.57	Ia
1999dk	UGC 1087	4181	5.3	-22.71(18)	11.67(110)	0.68(04)	1.26(06)	0	0.30	0.33	IaH
1999do	MCG+05-54-3	6238	4.7	-23.36(12)	5.42(106)	0.36(07)	Ia
1999dq	NGC 976	4060	4.1	-24.65(16)	11.97(097)	0.19(01)	1.07(02)	0.85	0.72	0.64	IaT
1999ej	NGC 495	3831	0.1	-23.66(17)	9.40(093)	0.82(05)	1.09(10)	0.28	0.22	0.22	IaN
1999ek	UGC 3329	5278	4.1	-24.71(13)	17.66(166)	0.63(21)	1.07(02)	IaN
2000A	MCG+01-59-8	12891	7.2	-24.80(07)	27.74(370)	0.16(02)	0.97(05)	IaN
2000B	NGC 2320	6020	-4.8	-25.76(11)	16.38(291)	0.56(09)	1.45(07)	IaH
...
2008hv	NGC 2765	4074	-1.9	-24.53(16)	15.47(136)	0.89(09)	1.10(10)	0	0.26	0.24	IaN

Note: The uncertainties shown in the parentheses are in units of 0.01 mag for M_K , 0.01 kpc for R_{gal} , 0.01 for relative distance, and 100 km s⁻¹ for Si II velocity.

*'Iabg' = 91bg-like SNe Ia; 'IaT' = 91T-like SNe Ia; 'IaN' = NV SNe Ia; 'IaH' = HV SNe Ia, 'IaPec' = 02cx-like SNe Ia; 'Ia' = unclassified SNe Ia.

The full data of Table S1 is available as a separate text file.